QT Variability and HRV Interactions in ECG: Quantification and Reliability

Rute Almeida* , Sónia Gouveia, Ana Paula Rocha, *Member, IEEE*, Esther Pueyo, Juan Pablo Martínez, and Pablo Laguna, *Senior Member, IEEE*

***Abstract*—In this paper, a dynamic linear approach was used over QT and RR series measured by an automatic delineator, to explore the interactions between QT interval variability (QTV) and heart rate variability (HRV). A low-order linear autoregressive model allowed to separate and quantify the QTV fractions correlated and not correlated with HRV, estimating their power spectral density measures. Simulated series and artificial ECG signals were used to assess the performance of the methods, considering a respiratory-like electrical axis rotation effect and noise contamination with a signal-to-noise ratio (SNR) from 30 to 10 dB. The errors found in the estimation of the QTV fraction related to HRV showed a nonrelevant performance decrease from automatic delineation. The joint performance of delineation plus variability analysis achieved less than 20% error in over 75% of cases for records presenting SNRs higher than 15 dB and QT standard deviation higher than 10 ms. The methods were also applied to real ECG records from healthy subjects where it was found a relevant QTV fraction not correlated with HRV (over 40% in 19 out of 23 segments analyzed), indicating that an important part of QTV is not linearly driven by HRV and may contain complementary information.**

***Index Terms*—Heart rate variability, modelling, QT interval, QT Variability, QT-RR interactions, RR interval.**

I. Introduction

THE electrocardiogram (ECG) analysis is extensively used as a diagnostic tool to provide information on the heart function. Each cardiac beat (Fig. 1) is typically associated with a sequence of six principal waves denoted by P, Q, R, S, T, and eventually U, whose characteristics are clinically relevant. In particular, the time interval between consecutive beats (RR interval) corresponds to the cardiac cycle duration and the time between the QRS complex onset and the T wave end (QT interval) represents the duration of the ventricular depolarization and repolarization phenomena.

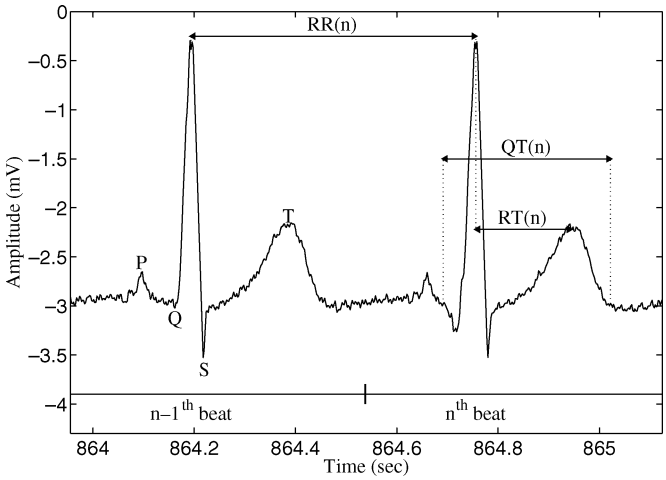

Fig. 1. Schematic representation of the five most common ECG waves and other relevant information in a cardiac beat.

The QT interval is currently considered as an index of the ventricular repolarization (VR) time, in spite of including the total (depolarization plus repolarization) ventricular electrical activity. Abnormal QT values have been associated with ventricular pro-arrhythmicity [1]–[3]. Lass *et al.* [4] studied VR dispersion assessed by RTapex or RTend intervals (respectively, the time between the R peak and T peak or end), which are alternatives to dispersion across leads. They found a strong correlation between level of myocardial electrical instability and RTend and RTapex time domain parameters (and other T wave based parameters). In a small group of patients with hypertrophic cardiomyopathy, Cuomo *et al.* [5] found abnormal QT beat-to-beat variations [QT interval variability (QTV)] both in time and frequency domain parameters, with the SDANN parameter [standard deviation (SD) of averaged QT on normal beats in 5-min segments] presenting a high predictive value for identifying patients with history of syncope. These findings support the idea that syncope in those patients may be related to repolarization changes. A normalized QTV index (QTVI = log ratio between the QT and HR variabilities, each normalized by its square mean) proposed in [6] and [7] allowed an improvement in the identification of cardiac arrest patients, compared to electrophysiologic test and other risk stratifiers. Increased QTVI has also been associated to life-threatening arrhythmia, sudden death in heart disease patients, and congestive cardiac failure in atrial fibrillation patients.

Despite the fact that VR length is extensively related with HR, several authors refer direct influences of autonomic nervous

Manuscript received June 15, 2005; revised December 18, 2005. This work was supported in part by the Ministerio de Ciencia y Tecnologia, Spain, and FEDER Grupo Consolidado GTC from DGA under Project TEC2004-05263-c02-02, and in part by the Fundação para a Ciência e Tecnologia (FCT), Portugal, through the programmes POCTI and POSI, with national and European Community Structural Funds (ESF), though Centro de Matemática da Universidade do Porto (CMUP). The work of R. Almeida and S. Gouveia was supported in part by the by FCT and ESF (Community Support Framework III) under Grant SFRH/BD/5484/2001 and Grant SFRH/BD/18894/2004. *Asterisk indicates corresponding author.*

*R. Almeida is with the Departamento de Matemática Aplicada, Faculdade de Ciências da Universidade do Porto (UP) and Centro de Matemática da UP (CMUP), Rua Campo Alegre 687, 4169-007 Porto, Portugal (e-mail: rbalmeid@fc.up.pt).

S. Gouveia and A. P. Rocha are with the Departamento de Matemática Aplicada, Faculdade de Ciências da Universidade do Porto (UP) and Centro de Matemática da UP (CMUP), 4169-007 Porto, Portugal (e-mail: sagouvei@fc.up.pt; aprocha@fc.up.pt).

E. Pueyo, J. P. Martínez, and P. Laguna are with the Communications Technology Group, Aragón Institute of Engineering Research (I3A), University of Zaragoza, 50018 Zaragoza, Spain (e-mail: epueyo@unizar.es; jpmart@unizar.es; laguna@unizar.es).

Digital Object Identifier 10.1109/TBME.2006.873682

system over VR [8]–[11] or report nonautonomic influences [12], [13]. In normal subjects, the direct effect of autonomic alterations over ventricular myocardium cells has been shown to change the QT in a way independent of heart rate (HR) [14]. Therefore, the QTV fraction not driven by the RR beat-to-beat variations [heart rate variability (HRV)] can itself have clinical meaning. Increased QTVI uncoupled with HRV was found during ischemic episodes [15] and dilated cardiomyopathy (ischemic and nonischemic) [16]; variations in QT versus RR interactions, possibly related with the high incidence of sudden death, were reported in heart failure patients [17].

The study of QTV requires the extraction of RR and QT intervals and, thus the ECG waves delineation. Besides the smaller amplitude of QTV compared to HRV, one of the main problems in studying this relation is the low amplitude and flat boundaries of the T waves, with consequent uncertainty in its end delineation. In clinical practice, noise contamination increases delineation difficulty and can result in spurious QTV. Some authors use alternative VR measures which do not require T wave end location, such as the RTapex interval. The use of the RTapex to assess VR is based on the assumption that the RR dependence of VR is concentrated on the early portion of the QT interval [18]. Porta *et al.* [19] studied the RR and RTapex intervals interactions, proposing a linear low-order dynamic parametric approach that allowed to quantify the fraction of the RTapex Variability (RTV) driven by HRV. The RTV was described as RR driven around the respiratory frequency and at low frequency (0.04–0.14 Hz), while a relevant RR-unrelated RTV fraction was found at lower frequencies. Using the same model, Lombardi *et al.* [20] reported a RTV fraction driven by HRV significantly greater in young subjects than in postmyocardial infaction patients and age matched control subjects. However, in spite of being easier to measure, RTapex presents even shorter length than QT interval and more reduced variability range. Moreover, the interval from T peak to T end (Tapex-end) was reported as RR independent in healthy subjects [21]. Variations of QT and QTapex were comparatively studied in normals, heart failure and ventricular hypertrophy situations: the terminal part of the T wave showed no HR dependence at rest and presented, both in exercise and in disease, substantial variability not related to QTapex variability. Furthermore, important abnormalities in QT interval, including HR-dependent ones, would be missed if the QTapex interval had been used to assess VR [21]. In fact, Yan *et al.* [22] stated that the interval Tapex-end represents transmural dispersion of VR and, thus may be considered as an arrhythmic risk index.

The QTV fraction effectively correlated with HRV has not been yet clearly quantified. In this paper, the QTV and HRV are assessed by the RR and QT intervals computed from automatic ECG delineation, thus avoiding intraobserver/interobserver variability. A wavelet transform based methodology previously validated [23] is used for that purpose. This system has proven to be quite robust against noise and morphological variations, even in the problematic T wave delineation. From the measured series, the QT and RR short term interactions are explored using a flexible orders version of the model proposed by Porta *et al.* [19], and the fraction of QTV driven by HRV is quantified. Preliminary versions of this methodology were partially validated in [24] and [25].

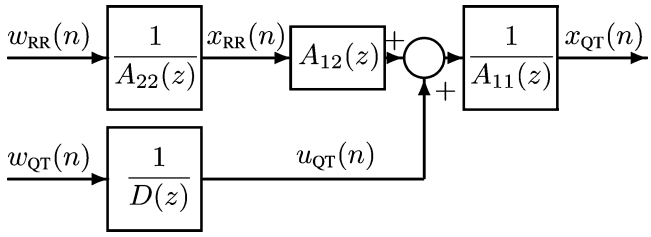

Fig. 2. Model of QTV versus HRV interactions.

The main aim of this paper is to establish the framework of applicability of the studied methods, giving the limits (as function of SNR and noise characteristics) to which the results can be reliable. The parametric approach is first validated in simulated series. The joint robustness of delineation and modelling is evaluated over artificial ECG signals, generated in a controlled situation, and facing respiratory and noise contamination. Application to real records is also presented. The parametric model formulation and identification are presented in Section II of this paper. The simulation set-up is described in Section III, along with the real data set. The performance evaluation can be found in Section IV. The results both in simulated and real data are presented in Section V and discussed in Section VI. Section VII comprises the conclusions.

II. Methods

The interval $RR(n)$ related to the nth beat is the time from $(n-1)$th to the nth beat, and $QT(n)$ refers to the QT interval in the nth beat (Fig. 1). The data to be analyzed by the parametric methodology are the interval series corrected for the mean, $x_{\mathrm{RR}}(n) = RR(n) - T_{\mathrm{R}}$ and $x_{\mathrm{QT}}(n) = QT(n) - T_{\mathrm{QT}}$, where T_{R} and T_{QT} stand for the mean RR and QT, respectively, in the analyzed segment.

A. Model Formulation and Spectral Decomposition

The parametric methodology explores QTV and HRV interactions assuming an open loop linear model [19] (Fig. 2) where $A_{11}(z)$, $A_{12}(z)$, $A_{22}(z)$ and $D(z)$ are polynomials with coefficients $a_{11}(k)$, $a_{12}(k)$, $a_{22}(k)$, and $d(k)$, respectively. The series $w_{\mathrm{RR}}(n)$ and $w_{\mathrm{QT}}(n)$ are uncorrelated stationary zero-mean white noises with SDs λ_{RR} and λ_{QT} and n denotes beat number. The series $x_{\mathrm{RR}}(n)$ is modelled as an order p autoregressive (AR_p) stationary random process

$$x_{\mathrm{RR}}(n) = -\sum_{k=1}^{p} a_{22}(k)x_{\mathrm{RR}}(n-k) + w_{\mathrm{RR}}(n). \qquad (1)$$

The QTV trend, $x_{\mathrm{QT}}(n)$, is assumed to result from two uncorrelated sources, one driven by HR and one resulting from other input (Fig. 2, ARARX_q model, [26])

$$\begin{aligned} x_{\mathrm{QT}}(n) &= -\sum_{k=1}^{q} a_{11}(k)x_{\mathrm{QT}}(n-k) \\ &\quad + \sum_{k=0}^{q} a_{12}(k)x_{\mathrm{RR}}(n-k) + u_{\mathrm{QT}}(n) \\ u_{\mathrm{QT}}(n) &= -\sum_{k=1}^{q} d(k)u_{\mathrm{QT}}(n-k) + w_{\mathrm{QT}}(n). \end{aligned} \qquad (2)$$

Therefore, the model accounts for the possible QT dependence on its past values and those of the RR interval. Recent studies evidenced these QT dependencies [27]. For simplicity, the same order q was assumed for all ARARX model polynomials, while a possibly different order p was allowed for the AR model. This is a generalization from previous approaches, where the same order was considered for all polynomials in the model ($p = q$) [19]. The order p in (1) represents the memory of $x_{\mathrm{RR}}(n)$ of its own past while order q in (2) produces a cumulative memory effect between the polynomials A_{11} and A_{22} or D, depending on the $x_{\mathrm{QT}}(n)$ dependence considered. Notice that $p = q$ corresponds to assigning to $x_{\mathrm{QT}}(n)$ series a double memory than to $x_{\mathrm{RR}}(n)$ series.

The assumption of uncorrelated sources allows to compute the power spectral density (PSD) of $x_{\mathrm{QT}}(n)$, $S_{\mathrm{QT}}(F)$, as the sum of the partial spectra, $S_{\mathrm{QT|RR}}(F)$ and $S_{\mathrm{QT|QT}}(F)$, that express the contributions related and unrelated to the RR interval, respectively

$$S_{\mathrm{QT|RR}}(F) = T_R \lambda_{\mathrm{RR}}^2 \left| \frac{A_{12}(z)}{A_{11}(z)A_{22}(z)} \right|^2_{z=e^{j2\pi F T_R}}$$

$$S_{\mathrm{QT|QT}}(F) = T_R \lambda_{\mathrm{QT}}^2 \left| \frac{1}{A_{11}(z)D(z)} \right|^2_{z=e^{j2\pi F T_R}}$$

where F is the frequency in Hz. As both $x_{\mathrm{QT}}(n)$ and $x_{\mathrm{RR}}(n)$ series are evenly sampled in beats but not in time, the mean RR interval (T_R) was used as sampling period for estimating the PSD functions, which has been shown acceptable for low frequencies far from the Nyquist frequency [28]. Each spectrum $S_{\mathrm{QT|E}}(F)$, $E \in \{RR, QT\}$ can be written as

$$\begin{aligned} S_{\mathrm{QT|E}}(F) &= T_R S_{\mathrm{QT|E}}(z)|_{z=e^{j2\pi F T_R}} \\ &= T_R \left[H_{\mathrm{QT|E}}(z) \lambda_E^2 H_{\mathrm{QT|E}}(z^{-1}) \right]_{z=e^{j2\pi F T_R}}. \end{aligned} \quad (3)$$

Factorizing $H_{\mathrm{QT|E}}(z)$ it is possible to decompose the complex spectral density in l_E components, each one referred to one of its poles $z_k, k = 1, \ldots, l_E$ [29] and [30]. Inverting the $\mathcal{Z}$-transform in the complex spectrum definition and computing the line integral using the *Cauchy Residue Theorem*, the autocorrelation function and the correspondent complex spectral density can be decomposed as $r_{\mathrm{QT|E}}(\tau) = \sum_{k=1}^{l_E} r_{\mathrm{QT|E}}^{(k)}(\tau)$ and $S_{\mathrm{QT|E}}(z) = \sum_{k=1}^{l_E} \mathcal{Z}\{r_E^{(k)}(\tau)\} = \sum_{k=1}^{l_E} S_{\mathrm{QT|E}}^{(k)}(z)$.

According to [30], each term in $S_{\mathrm{QT|E}}(z)$ can be written as

$$S_{\mathrm{QT|E}}^{(k)}(z) = \frac{\gamma_k z_k}{(z^{-1} - z_k)} + \gamma_k + \frac{\gamma_k z_k}{(z - z_k)}$$

for $\gamma_k = \mathrm{Res}[S_{\mathrm{QT|E}}(z)/z]$, calculated at $z = z_k$. Since the residues for complex conjugate poles are complex conjugate, the total power in the spectrum can be written as the sum of $g_{\mathrm{E}} \leq l_{\mathrm{E}}$ components: one for each pair of complex conjugate poles z_g and z_g^* (located at frequencies F_g and $-F_g$) and one for each real pole z_g (at $F_g = 0$ or $F_g = 1/(2T_R)$), if they exist. That is

$$\begin{aligned} r_{\mathrm{QT|E}}(0) &= \sum_{k=1}^{l_E} \gamma_k \\ &= \sum_{\substack{g \\ 0 < F_g < \frac{1}{2T_R}}} \left(\gamma_g + \gamma_g^*\right) + \sum_{\substack{g \\ F_g \in \left\{0, \frac{1}{2T_R}\right\}}} \gamma_g. \end{aligned} \quad (4)$$

Due to the symmetry of $S_{\mathrm{QT|E}}(F)$ with respect to $F = 0$, frequencies associated to complex conjugate poles correspond to complex conjugate components that can be combined in a real $S_{\mathrm{QT|E}}^{(g)}(F)$, related to a power component $\gamma_g + \gamma_g^* = 2\Re(\gamma_g)$ [29]. Each term γ_g in the last sum of (4) can be seen as the power of a real component $S_{\mathrm{QT|E}}^{g}(F)$ corresponding to $F_g = 0$ or $F_g = 1/(2T_R)$ (that is, for z_g real). Therefore, $S_{\mathrm{QT|E}}(F)$ in (3) can be decomposed into components $S_{\mathrm{QT|E}}^{(g)}(F)$, contributing mainly at frequencies $0 \leq F_g \leq 1/(2T_R)$. The power within a given frequency band, $\mathcal{B}$ denoted by $P_{\mathrm{QT|E}}^{\mathcal{B}}$, can be obtained by summing the contributions of the poles located in the band $\mathcal{B}$. That is

$$P_{\mathrm{QT|E}}^{\mathcal{B}} = \sum_{\substack{g \\ F_g \in \mathcal{B}}} c_g \Re(\gamma_g)$$

where $c_g = 1$ for real poles and $c_g = 2$ for complex conjugate poles. The relative fraction of the QTV driven by RR in the frequency band $\mathcal{B}$ is given by

$$R_{\mathrm{QT|RR}}^{\mathcal{B}} = \frac{P_{\mathrm{QT|RR}}^{\mathcal{B}}}{P_{\mathrm{QT|RR}}^{\mathcal{B}} + P_{\mathrm{QT|QT}}^{\mathcal{B}}} \times 100. \quad (5)$$

This algebraic decomposition of the spectrum does not guarantee the achievement of admissible spectral components, once negative power components can occur, if poles are too close together [31]. If this happens near the limit of a frequency band $\mathcal{B}$, a negative $P_{\mathrm{QT|E}}^{\mathcal{B}}$ value can be obtained and protection rules need to be considered in the estimation, as will be explained in the next section.

B. Model Identification and Order Selection

From $x_{\mathrm{RR}}(n)$ and $x_{\mathrm{QT}}(n)$ interval series, the polynomial A_{22} was estimated using least squares, while the ARARX model parameters were iteratively obtained using a generalized least squares methodology [26]. A large enough signal-to-noise ratio (SNR) guarantees that the minima of the square residue are global [26] and convergence to white noise residuals $w_{\mathrm{QT}}(n)$ is expected in a reasonable small number of iterations for adequate model orders.

Orders p, q between 2 and 18 were considered to be adequate for modelling a given data segment if the residuals $w_{\mathrm{RR}}(n)$ and $w_{\mathrm{QT}}(n)$ can be considered uncorrelated white noises (5% significance bilateral test on the normalized autocorrelations and crosscorrelation, both for the first 40 lags and for all lags). Model orders producing a negative global contribution in a frequency band, as remarked in Section II-A, were also considered as inadequate. Optimal p and q were automatically selected from the adequate orders. First, order p of A_{11} in the AR model is chosen by minimizing the Akaike information criteria (AIC) [26]. The order q is taken as the one minimizing the multivariate AIC

$$\log\left(det(\mathbf{\Sigma})\right) + 2 * (p + 3q + 1)/N \quad (6)$$

where $det(\mathbf{\Sigma})$ stands for the determinant of the covariance matrix of the residuals $w_{\mathrm{RR}}(n)$ and $w_{\mathrm{QT}}(n)$, and N is the number of intervals (beats) in the segment. The order p, and therefore the

$w_{\mathrm{RR}}(n)$ variance, were already determined in the previous step, and thus this is not a multivariate minimization in strict sense, as only the q order remains to be chosen. To reduce overfit problems in AIC, the number of estimated parameters $(p+3q+1)$ should be small (less that 10%) with respect to the total number of intervals in the series [32]. Regarding the extreme case $p = q = 18$, segments with a minimum of about 350 beats should be considered.

III. Data Sets

Test data was simulated for validation of the previously described methodology. The $x_{\mathrm{RR}}(n)$ and $x_{\mathrm{QT}}(n)$ series were simulated using the linear relations model (Fig. 2) and artificial ECG signals matching those intervals were constructed to evaluate the methodology in a more realistic context. Along with morphologic beat-to-beat variability, real ECG signals are also affected by extra cardiac factors, such as respiration or muscular activity, which have also been considered in the simulation. Real ECG records from a database were used to illustrate the method in clinical practice.

A. Simulated Data

Assuming that the linear model in Fig. 2 holds, it is necessary to define reference parameters for $x_{\mathrm{QT}}(n)$ series generation in controlled simulation. Aiming to obtain realistic $x_{\mathrm{QT}}(n)$ resulting from $x_{\mathrm{RR}}(n)$ and an uncorrelated source $w_{\mathrm{QT}}(n)$, in a first step were constructed the series

$$x_{\mathrm{QT}}(n) = a\left(\sqrt{x_{\mathrm{RR_{Re}}}(n)} + \sqrt{x_{\mathrm{RR_{Ti}}}(n)}\right) + b \qquad (7)$$

from which the reference model parameters are going to be extracted. The series $x_{\mathrm{RR_{Re}}}(n)$ and $x_{\mathrm{RR_{Ti}}}(n)$ are independent $x_{\mathrm{RR}}(n)$ realizations obtained using an integral pulse frequency modulation model, following AR_7 modulating signals [28], agreeing to the spectra typically found at supine rest and head-up tilt situations, respectively (Fig. 3, upper left corner) [33]. The RR uncorrelated QTV part does not need to have a RR like spectral shape, as has been here considered. However, this choice assigns to the uncorrelated part a spectral behaviour which puts the method under evaluation in the more difficult situation, that is with the same kind of frequency distribution as in the RR. So, the spectral overlap will force the method to search for uncorrelations rather than just make frequency filtering. The parameters b and a in (7) allow to set $x_{\mathrm{QT}}(n)$ mean and SD (σ_{QT}) and adjusting a is equivalent to consider distinct QTV levels. Parametric model identification in (1) and (2), considering $x_{\mathrm{RR}}(n) = x_{\mathrm{RR_{Re}}}(n)$ and $x_{\mathrm{QT}}(n)$ given by (7) provides the reference coefficients values $a^r_{12}(k)$, $a^r_{11}(k)$, $d^r(k)$, and the residual noise SD λ^r_{QT} for the simulation. The QT reference models construction is summarized in the upper block of the diagram in Fig. 3. In this study, two different QTV levels $Hi(\sigma_{\mathrm{QT}} = 17\ \mathrm{ms})$ and $Lo(\sigma_{\mathrm{QT}} = 5\ \mathrm{ms})$ were modelled, which were chosen to express extreme situations found in healthy subjects [34]. In order to allow a better spanning of the QTV level range, additional QT reference models were also constructed for $\sigma_{\mathrm{QT}} = 13$, 10, 8, and 3 ms. The order $q = 4$ was chosen to include similar memory ($2q = 8$, $p = 7$) on its own past for both $x_{\mathrm{QT}}(n)$ and $x_{\mathrm{RR}}(n)$, while $x_{\mathrm{QT}}(n)$ depends on $p+q$ past $x_{\mathrm{RR}}(n)$ samples.

Once the QT reference model parameters were obtained, the test data was simulated as outlined in the central block of Fig. 3. The $x_{\mathrm{QT}}(n)$ fraction driven by RR, $x_{\mathrm{QT|RR}}(n)$, was obtained by feeding the correspondent part of the model (Fig. 2) with independent realizations of $x_{\mathrm{RR}}(n)$

$$x_{\mathrm{QT|RR}}(n) = -\sum_{k=1}^{q} a^r_{11}(k)x_{\mathrm{QT|RR}}(n-k) + \sum_{k=0}^{q} a^r_{12}(k)x_{\mathrm{RR}}(n). \qquad (8)$$

Analogously, $u_{\mathrm{QT}}(n)$ and the fraction noncorrelated with RR $(x_{\mathrm{QT|QT}}(n))$ were obtained feeding with simulated white noise (SD λ^r_{QT}), $w_{\mathrm{QT}}(n)$

$$x_{\mathrm{QT|QT}}(n) = u_{\mathrm{QT}}(n) - \sum_{k=1}^{q} a^r_{11}(k)x_{\mathrm{QT|QT}}(n-k);$$

$$u_{\mathrm{QT}}(n) = -\sum_{k=1}^{q} d^r(k)u_{\mathrm{QT}}(n-k) + w_{\mathrm{QT}}(n). \qquad (9)$$

Fifty uncorrelated realizations (trials) of more than 1000 beats were simulated regarding the following three cases of possible *dependencies*.

A) QT and RR fully correlated: $x_{\mathrm{QT}}(n) = x_{\mathrm{QT|RR}}(n)$.
B) QT and RR uncorrelated: $x_{\mathrm{QT}}(n) = x_{\mathrm{QT|QT}}(n)$.
C) Mixture of the two dependencies

$$x_{\mathrm{QT}}(n) = x_{\mathrm{QT|RR}}(n) + x_{\mathrm{QT|QT}}(n).$$

Several simulation approaches were then considered and different test data sets were obtained, as summarized in Table I. The *clean simulated* test data sets ("c") were defined from the series simulated directly from each reference model, considering the three dependence cases. Artificial ECG signals were constructed based on those series and were used to obtain *signal derived* data sets. The interval measurements from the marks provided by automatic delineation of those noncontaminated ECGs led, for each dependence case, a new data set ("s"). Different contamination types were considered by including a *respiratory-like electrical axis rotation effect* ("r") or adding real *prerecorded noise* ("v") to the ECG signals in the dependence case C. These test data sets are further described next.

1) Clean Series Simulation: A segment of 350 beats from every realization of the series simulated directly from each reference model were considered in test data, defining the *clean* test data sets ("c"), respectively, A_c, B_c, and C_c.

2) Signal Derived Series: Artificial ECG signals were constructed fitting the previously generated $x_{\mathrm{RR}}(n)$ and $x_{\mathrm{QT}}(n)$ series in each data set. A clean and well defined template beat was chosen from a 3-lead baseline corrected real file, sampled at 500 Hz, the same resolution than the real data (see Section III-B). Each ECG was obtained by concatenation of the template beat, following the $x_{\mathrm{RR}}(n)$ series, properly scaled from QRS end to T wave end to reflect the variability inherent to $x_{\mathrm{QT}}(n)$. By applying the same scaling to template beats from the orthogonal leads X, Y and Z, 3-lead artificial ECG signals with same QTV and HRV in all leads $(y^L(k), L \in \{X, Y, Z\})$ can be obtained. Automatic delineation over these signals [23] provided

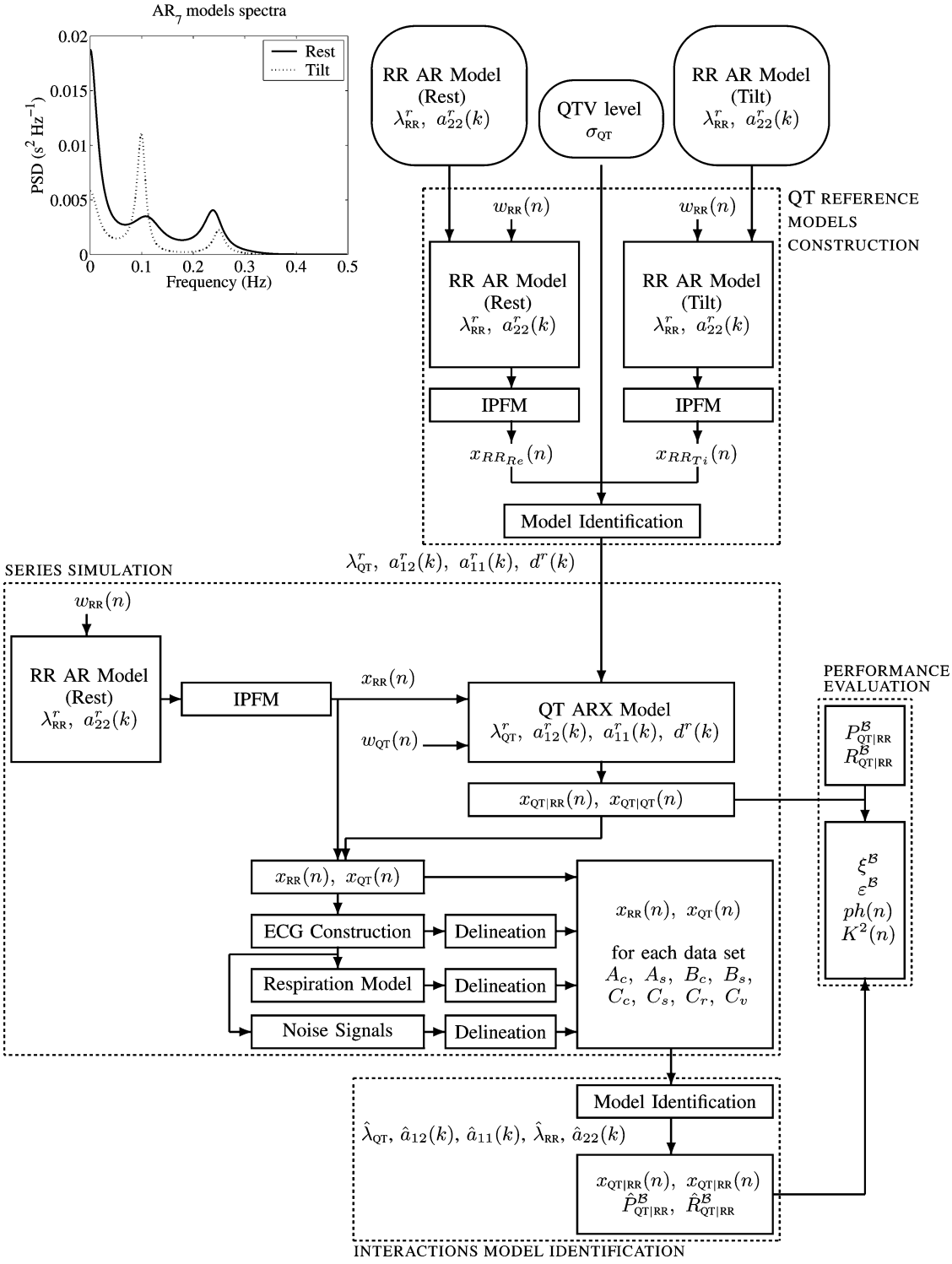

Fig. 3. Methods block diagram: QT reference models construction (upper block), test data sets simulation (central block), QTV versus HRV interactions model estimation (lower block), performance evaluation (right side).

the fiducial marks and the corresponding series $x_{\mathrm{RR}}(n)$ and $x_{\mathrm{QT}}(n)$ *signal derived* ("s") were checked for RR outliers [35] and missing QT values. Segments of consecutive 350 valid beats measures were considered and denoted as data sets A_s, B_s, and C_s.

3) Noise Contamination: Different contamination types were considered over the 50 trials in the situation of mixture of dependencies (case C), as illustrated in Fig. 4. A *respiratory-like electrical axis rotation effect* ("r") was simulated and the data set C_r was constructed from the series of automatically delineated intervals over the ECG signal affected by respiratory noise. Other contamination types were considered by adding prerecorded noise to the artificial ECG and a new data set C_v was defined from the $x_{\mathrm{RR}}(n)$ and $x_{\mathrm{QT}}(n)$ series obtained

TABLE I
SIMULATED DATA: MEAN AND SD OF $\hat{\sigma}_{\mathrm{QT}}$ IN VALID SEGMENTS (ms). (NC: NOT CONSIDERED)

				QT reference model			
				Hi ($\sigma_{\mathrm{QT}} = 17$ ms)		*Lo* ($\sigma_{\mathrm{QT}} = 5$ ms)	
Test data	Dependency case	Dataset	#	mean	sd	mean	sd
Clean simulated series	A	A_c	50	13.5	0.8	4.1	0.3
	B	B_c	50	9.1	0.7	3.0	0.3
	C	C_c	50	16.4	1.1	5.1	0.4
Signal derived series: no noise contamination	A	A_s	50	12.7	0.7	4.1	0.2
	B	B_s	50	8.7	0.6	3.0	0.3
	C	C_s	50	15.4	1.0	5.1	0.3
pre-recorded noise	A	NC					
	B	NC					
	C	C_v(30 dB)	150	15.5	1.0	5.2	0.4
		C_v(25 dB)	150	15.7	1.0	5.7	0.6
		C_v(20 dB)	150	15.8	1.0	6.1	0.7
		C_v(15 dB)	150	16.8	1.4	8.1	1.8
respiratory-like effect	A	NC					
	B	NC					
	C	C_r	50	15.4	1.0	5.4	0.3

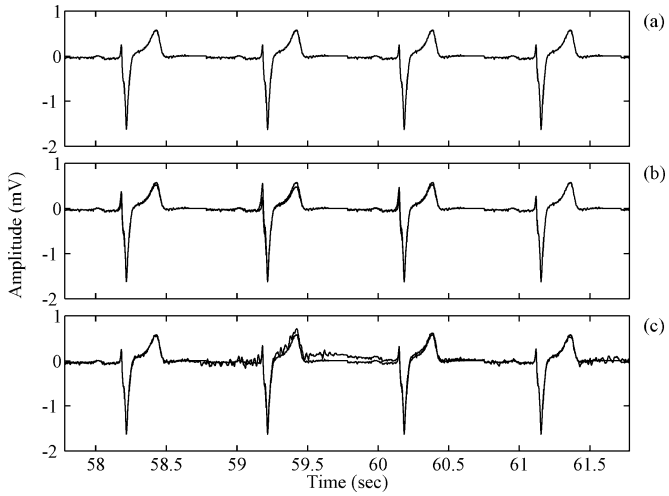

Fig. 4. Example of (a) a simulated ECG signal, (b) the same ECG with noise contamination (thicker line) with respiratory-like electrical axis rotation effect, and (c) muscular artifacts with $\mathrm{SNR} = 15$ dB. Clean ECG superimposed (thinner line) in (b) and (c).

from the delineation over these *noisy* ("v") ECGs. Outliers and missing values can occur due to misdetection in automatic delineation. After delineation, all potential RR outliers were excluded [35] and segments of consecutive 350 valid beats measures considered in the test data sets.

Lungs expansion and contraction during the respiratory cycle changes the heart electric axis within the chest, resulting in scaling and rotation on the ECG. It is assumed that the angular variation around a lead axis is a function of the amount of air in the lungs at each time, which was modelled as a sinusoid. The rotation angle around each orthogonal lead $L \in \{X, Y, Z\}$ is given by

$$\varphi^L(k) = 0.5\phi^L \left(sin\left(2\pi k \frac{F_r}{F_s}\right) + 1 \right) \tag{10}$$

where k is sample index, ϕ^L is the maximum value allowed for $\varphi^L(k)$, and F_r and F_s denote respiratory and sampling frequency, respectively. The rotation matrix $Q(k)$ can be computed as the product of planar rotations with angles $\varphi^L(k)$ and the effect of a three lead rotation should not be different than along one single lead [36]. For the sake of simplicity, only the rotation around the Z axis was considered with $\phi^Z = 15\pi/180$ rad. The respiratory frequency was set to $F_r = 0.24$ Hz, corresponding to the central frequency of the highest variability peak on the $x_{RR_{Re}}(n)$ model spectra (Fig. 3). The ECG signals affected by respiration $[y_r^X(k) y_r^X(k) y_r^Z(k)]$ were constructed as the product of $Q(k)$ matrix by the 3-lead ECG vector $[y^X(k) y^Y(k) y^Z(k)]$.

Prerecorded noise from the MIT-BIH Noise Stress Test Database [37] was used, corresponding to baseline wandering, electrode movement artifacts and muscular artifacts. The first lead of the noise records was resampled at 500 Hz and multiplied by a constant to get a predefined SNR (levels from 30 dB to 5 dB) when added to the artificial ECG. The data set C_v comprehends the $x_{\mathrm{RR}}(n)$ and $x_{\mathrm{QT}}(n)$ series obtained from the contaminated ECGs considering all noise types and SNR levels.

B. Real Data Set

ECG recordings of young normal subjects from POLI/MEDLAV database [38] were used in this study (20 records 24 min long sampled at 500 Hz with X, Y, and Z leads). Each lead was processed by the automatic delineation system [23]. In addition to all potential RR outliers [35], QT intervals out of a 3-SD band were also rejected, as they are unlikely to be physiologically meaningful and must have resulted from error in delineation. In the subsequent analysis, segments of 350 consecutive beats with valid RR and QT intervals measurements were considered. Longer segments were carved up. Each qualified segment was evaluated for the QT variability level (estimated as the QT SD) and SNR level (estimated as the ratio between the power of a running averaged and amplitude fitted beat and the power of a segment between QRS complexes high-pass filtered with a fifth-order Butterworth filter with cut-off frequency 10 Hz).

IV. Performance Evaluation

The actual spectra of the simulated series was obtained directly from the reference parameters in each QT reference model given in Section III-A, used to generate the simulated series. The spectral decomposition was performed as described in Section II-A and the reference variability measures $P^{\mathcal{B}}_{\mathrm{QT|RR}}$ calculated. The errors $\xi^{\mathcal{B}}$ in the estimated variability measures $\hat{P}^{\mathcal{B}}_{\mathrm{QT|RR}}$ are computed as

$$\xi^{\mathcal{B}} = \hat{P}^{\mathcal{B}}_{\mathrm{QT|RR}} - P^{\mathcal{B}}_{\mathrm{QT|RR}}. \tag{11}$$

The QTV fraction driven by HRV was chosen as a performance measure since it is more likely to be correctly estimated, due to the fact that any spurious QTV will be considered as part of the uncorrelated fraction. The percentage errors $\varepsilon^{\mathcal{B}}$ in the quantification of the QTV fraction correlated with HRV are defined as the difference between the ratios calculated from (5) for estimated, $\hat{R}^{\mathcal{B}}_{\mathrm{QT|RR}}$, and reference measures, $R^{\mathcal{B}}_{\mathrm{QT|RR}}$

$$\varepsilon^{\mathcal{B}} = \hat{R}^{\mathcal{B}}_{\mathrm{QT|RR}} - R^{\mathcal{B}}_{\mathrm{QT|RR}}. \tag{12}$$

The percentage errors $\varepsilon^{\mathcal{B}}$ depend on both QTV fractions and thus are more sensitive performance indicators than the errors $\xi^{\mathcal{B}}$, since overestimated $P^{\mathcal{B}}_{\mathrm{QT|QT}}$ leads to an artificial decrease on $R^{\mathcal{B}}_{\mathrm{QT|RR}}$.

From the estimated coefficients and the residues $\hat{w}_{\mathrm{RR}}(n)$ and $\hat{w}_{\mathrm{QT}}(n)$, the signals $\hat{x}_{\mathrm{QT|RR}}(n)$ and $\hat{x}_{\mathrm{QT|QT}}(n)$, corresponding to the $x_{\mathrm{QT}}(n)$ fractions, were explicitly calculated. The similarity between $\hat{x}_{\mathrm{QT|RR}}(n)$ and the corresponding simulated series $x_{\mathrm{QT|RR}}(n)$ in (8) was evaluated by the magnitude of the squared spectral coherence $K^2(F)$ and the phase of the cross-spectra $ph(F)$, obtained by bivariate AR_7 modelling [31]. Analogously, $\hat{x}_{\mathrm{QT|QT}}(n)$ and $x_{\mathrm{QT|QT}}(n)$ in (9) were also compared.

V. Results

The measures were estimated considering frequency bands typically used in HRV studies [33]: low-frequency ($\mathcal{B} = \mathrm{LF}$) as 0.04–0.15 Hz and high-frequency ($\mathcal{B} = \mathrm{HF}$) as 0.15–0.4 Hz. Total power ($\mathcal{B} = \mathrm{TP}$) was taken from 0.04 Hz to the highest frequency present in each spectrum $1/(2T_R)$.

A. Simulated Data

Both for the directly simulated data sets (A_c, B_c, C_c), and the ones obtained by automatic delineation without noise contamination (A_s, B_s, C_s) no potential RR outliers or missing QT intervals occurred. Adequate segments (350 consecutive beats and no potential RR outliers) were also found in all 50 trials of data sets C_r and C_v for $\mathrm{SNR} \geq 15$ dB for all QT reference models. The reduced number of qualified segments led us to exclude data with $\mathrm{SNR} \leq 10$ dB from the analysis. The estimated QT SD, $\hat{\sigma}_{\mathrm{QT}}$, in the valid segments of each data set obtained from QT reference models Hi and Lo are reported in Table I ($\hat{\sigma}_{\mathrm{QT}}$ mean and SD across trials).

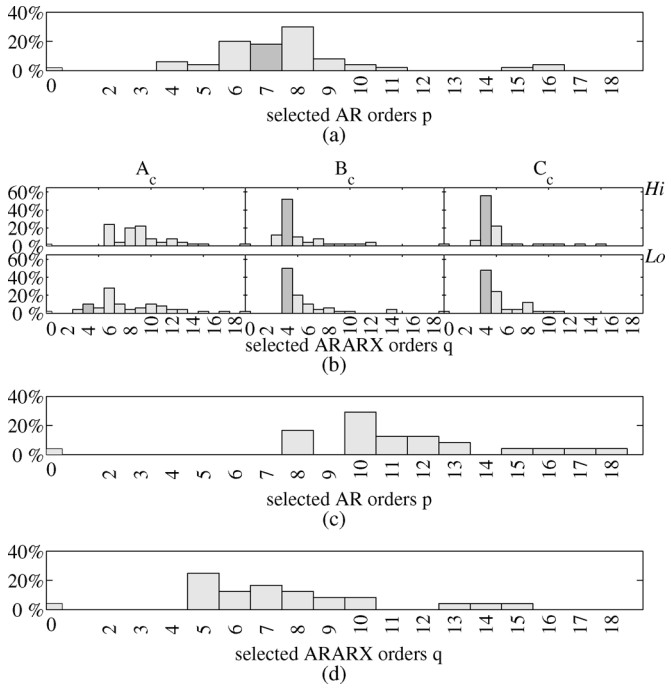

Fig. 5. Histograms of orders p and q selected by AIC in model identification for (a) clean RR simulated series and (b) clean QT simulated series with QT reference models Hi and Lo, and (c) and (d) real data set segments. Darker classes in (a) and (b) corresponds to the reference order.

A minimum of 48 (out of 50) valid estimated models for each QT reference model were found for every data set and noise type in data set C_v for SNR level $\geq$15 dB.

1) Clean Simulated Series: The AIC selected orders for the AR model are presented in Fig. 5(a), with $5 \leq p \leq 9$ in 82% of the cases. For the ARARX model, AIC selected orders $3 \leq q \leq 7$ in more than 80% of the series in data sets B_c and C_c for all QT reference models, while more spread orders were selected for data set A_c, as illustrated in Fig. 5(b) for QT reference models Hi and Lo.

For QT reference models Hi and Lo, the mean and SD of $\xi^{\mathcal{B}}(\overline{\xi}^{\mathcal{B}}, s^{\mathcal{B}}_{\xi})$ are presented in Table II(a) for data sets A_c and B_c; the mean and SD of $\varepsilon^{\mathcal{B}}(\overline{\varepsilon}^{\mathcal{B}}, s^{\mathcal{B}}_{\varepsilon})$ are also presented in Table II(a) for data sets A_c and B_c and in Table II(b) for data set C_c. In all cases for QT reference models with $\sigma_{\mathrm{QT}} \geq 5$ ms, $\overline{\varepsilon}^{\mathrm{HF}} \leq 5.1\%(s^{\mathrm{HF}}_{\varepsilon} \leq 5.5\%)$, $\overline{\varepsilon}^{\mathrm{LF}} \leq 3\%(s^{\mathrm{LF}}_{\varepsilon} \leq 10.1\%)$ and $\overline{\varepsilon}^{\mathrm{TP}} \leq 3.5\%(s^{\mathrm{TP}}_{\varepsilon} \leq 7\%)$. The distributions of $\varepsilon^{\mathcal{B}}$ for QT reference models Hi and Lo in datasets A_c, B_c and C_c are presented in Fig. 6(a). In this chart, and in all similar ones, the central box goes from 1st to 2nd quartiles, with a horizontal line marking the median, and + stands for values out of the quartiles box. Considering QT reference models corresponding to $\sigma_{\mathrm{QT}} \geq 8$ ms, $\epsilon^{\mathcal{B}} < 5\%$ for more than 81% of the series with $\mathcal{B} = \{\mathrm{TP}, \mathrm{HF}\}$, and 78% with $\mathcal{B} = \mathrm{LF}$. For QT reference model Lo, $\epsilon^{\mathcal{B}} < 5\%$ for 78% with $\mathcal{B} = \mathrm{TP}$ (74% with $\mathcal{B} = \mathrm{LF}$, 71% with $\mathcal{B} = \mathrm{HF}$). The comparison between estimated and reference fractions, regarding both $\hat{x}_{\mathrm{QT|RR}}(n)$ and $\hat{x}_{\mathrm{QT|QT}}(n)$ were evaluated across trials (Fig. 7). The magnitude of the squared coherence $K^2(F)$ was found to be higher in the QTV fraction driven by RR than in the uncorrelated one. For QT reference models with lower σ_{QT},

TABLE II
MEAN AND SD OF ERRORS $\varepsilon^{\mathcal{B}}$ and $\xi^{\mathcal{B}}$ IN (a) DATASETS A_c, B_c, A_s, B_s AND $\varepsilon^{\mathcal{B}}$ AND IN (b) DATASETS C_c, C_s, C_r, AND C_v FOR $\mathrm{SNR} \geq 15$ dB

(a)

		$\bar{\varepsilon}^{\mathcal{B}} \pm s_{\varepsilon}^{\mathcal{B}}, \%$				$\xi^{\mathcal{B}} \pm s_{\xi}^{\mathcal{B}}, \%$			
	$\mathcal{B}$	A_c	B_c	A_s	B_s	A_c	B_c	A_s	B_s
QT reference model Hi	TP	-0.4 ± 0.1	2.0 ± 1.6	-0.7 ± 0.2	2.3 ± 1.8	-7.0 ± 18.9	1.4 ± 1.1	-0.7 ± 0.2	2.3 ± 1.8
	LF	-0.2 ± 0.1	1.9 ± 2.0	-0.4 ± 0.2	2.1 ± 2.2	0.8 ± 17.2	1.0 ± 1.1	-0.4 ± 0.2	2.1 ± 2.2
	HF	-0.5 ± 0.1	2.6 ± 2.3	-0.9 ± 0.2	3.0 ± 2.4	-7.8 ± 6.4	0.3 ± 0.3	-0.9 ± 0.2	3.0 ± 2.4
QT reference model Lo	TP	-3.5 ± 0.7	2.7 ± 2.7	-3.5 ± 0.7	2.7 ± 2.7	-0.5 ± 1.7	0.2 ± 0.2	-3.5 ± 0.7	2.7 ± 2.7
	LF	-2.0 ± 0.9	2.8 ± 3.5	-2.0 ± 0.8	2.8 ± 3.5	0.1 ± 1.6	0.2 ± 0.2	-2.0 ± 0.8	2.8 ± 3.5
	HF	-4.6 ± 1.1	2.2 ± 1.8	-4.7 ± 1.2	2.2 ± 1.8	-0.6 ± 0.5	0.0 ± 0.0	-4.7 ± 1.2	2.2 ± 1.8

(b)

		$\bar{\varepsilon}^{\mathcal{B}} \pm s_{\varepsilon}^{\mathcal{B}}, \%$						
	$\mathcal{B}$	C_c	C_s	$C_{v(30\ \mathrm{dB})}$	$C_{v(25\ \mathrm{dB})}$	$C_{v(20\ \mathrm{dB})}$	$C_{v(15\ \mathrm{dB})}$	C_r
QT reference model Hi	TP	-1.5 ± 5.5	-1.7 ± 6.4	-2.7 ± 6.7	-3.9 ± 6.9	-5.8 ± 7.4	-12.5 ± 9.3	-3.0 ± 6.4
	LF	-0.1 ± 7.7	-0.2 ± 9.2	-0.9 ± 9.9	-1.1 ± 10.3	-2.7 ± 11.6	-5.4 ± 11.7	0.3 ± 9.3
	HF	-1.9 ± 4.3	-2.0 ± 4.5	-4.2 ± 5.0	-8.4 ± 6.8	-11.8 ± 7.1	-24.4 ± 11.5	9.2 ± 5.2
QT reference model Lo	TP	-1.9 ± 7.0	-2.1 ± 7.1	-6.6 ± 7.7	-15.8 ± 11.4	-22.4 ± 11.3	-36.7 ± 9.5	-16.8 ± 6.5
	LF	0.2 ± 9.8	0.1 ± 9.9	-0.9 ± 10.2	-6.4 ± 12.3	-12.4 ± 12.5	-24.5 ± 15.6	0.0 ± 11.5
	HF	-5.1 ± 5.5	-5.6 ± 5.7	-15.8 ± 8.7	-29.3 ± 15.5	-36.4 ± 14.1	-49.7 ± 15.1	-39.9 ± 6.1

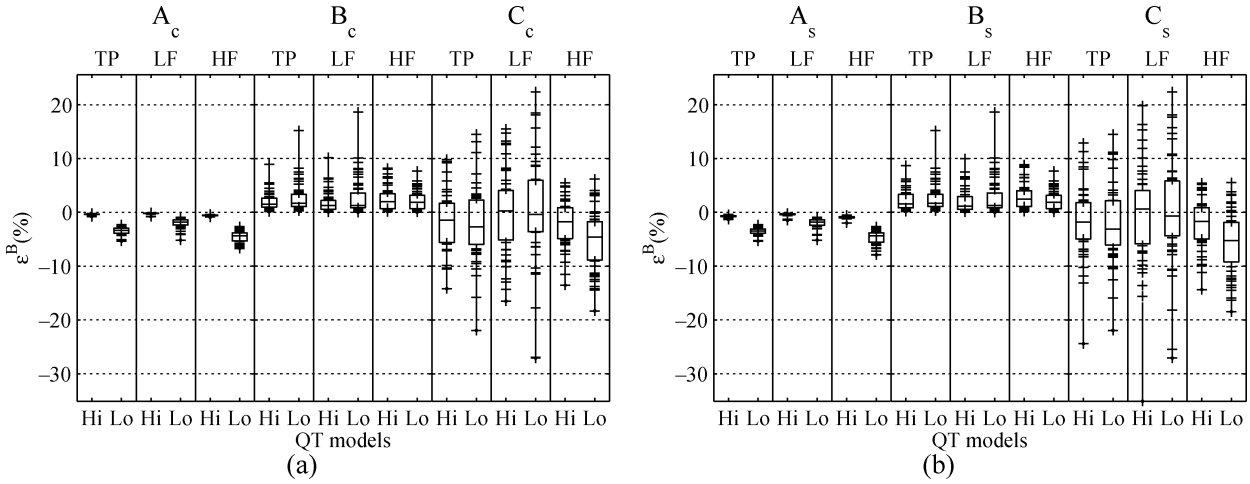

Fig. 6. Distributions of $\varepsilon^{\mathcal{B}}$ in (a) data sets A_c, B_c, C_c and (b) data sets A_s, B_s, C_s: box-and-whisker plot by frequency band (+ stands for values out of the quartiles box).

$K^2(F)$ decreased and both $K^2(F)$ and $ph(F)$ became more spread in both QTV fractions.

2) Signal Derived Series: For QT reference models with $\sigma_{\mathrm{QT}} \geq 8$ ms, $\epsilon^{\mathcal{B}} < 5\%$ in more than 80% of the series for $\mathcal{B} = \mathrm{HF}$, and 76% for $\mathcal{B} = \{\mathrm{LF}, \mathrm{TP}\}$. For QT reference model Lo, $\epsilon^{\mathcal{B}} < 5\%$ for about 76% with $\mathcal{B} = \mathrm{TP}$ (75% with $\mathcal{B} = \mathrm{LF}$, 66% with $\mathcal{B} = \mathrm{HF}$). In all the cases for QT reference models with $\sigma_{\mathrm{QT}} \geq 5$ ms, $\bar{\varepsilon}^{\mathrm{HF}} \leq 5.7\%(s_{\varepsilon}^{\mathrm{HF}} \leq 6.3\%)$, $\bar{\varepsilon}^{\mathrm{LF}} \leq 3\%(s_{\varepsilon}^{\mathrm{LF}} \leq 10\%)$ and $\bar{\varepsilon}^{\mathrm{TP}} \leq 3.6\%(s_{\varepsilon}^{\mathrm{TP}} \leq 7.6\%)$. For QT reference models Hi and Lo, the values of $\bar{\varepsilon}^{\mathcal{B}} \pm s_{\varepsilon}^{\mathcal{B}}$ and $\bar{\xi}^{\mathcal{B}} \pm s_{\xi}^{\mathcal{B}}$ in data sets A_s and B_c, and $\bar{\varepsilon}^{\mathcal{B}} \pm s_{\varepsilon}^{\mathcal{B}}$ for data set C_s can be found in the Tables II(a) and II(b) and $\varepsilon^{\mathcal{B}}$ distribution in Fig. 6(b). The $K^2(F)$ and $ph(F)$ obtained were equivalent to the clean series data sets results.

3) Noise Contamination: The distribution of ξ^{LF} and ξ^{HF} in data sets C_v and C_r is presented in Fig. 8(a). Larger bias was found for $\mathcal{B} = \mathrm{HF}$ and higher dispersion for $\mathcal{B} = \mathrm{LF}$. A reduction in ξ^{B} bias and dispersion was observed with QTV level reduction, however both increased proportionally to $P^{\mathcal{B}}_{\mathrm{QT|RR}}$. No relevant effect was noticed from the respiratory-like contamination considered. The distributions of $\varepsilon^{\mathrm{LF}}$ and $\varepsilon^{\mathrm{HF}}$ are presented in Fig. 8(b); $\bar{\varepsilon}^{\mathcal{B}} \pm s_{\varepsilon}^{\mathcal{B}}$ values can be found in Table II(b). Noise and respiratory-like contamination produced a negative bias, specially marked in for $\mathcal{B} = \mathrm{HF}$. Both bias and dispersion of $\varepsilon^{\mathcal{B}}$ were more evident with QT reference models corresponding to lower σ_{QT} and had progressively increased with noise contamination (lower SNR values). This performance decay reached important levels for $\mathrm{SNR} \leq 20$ dB with, $\sigma_{\mathrm{QT}} \leq 3$ ms for $\mathcal{B} = \mathrm{LF}$ and $\sigma_{\mathrm{QT}} \leq 5$ ms for $\mathcal{B} = \mathrm{HF}$, and for respiratory contamination with $\sigma_{\mathrm{QT}} \leq 10$ ms for $\mathcal{B} = \mathrm{HF}$. Considering separately the different noise types, no relevant differences were found between baseline wandering and muscular artifacts contamination. The method was slightly more robust to electrode movement artifacts contamination with intermediate SNR levels (lower $\xi^{\mathcal{B}}$ bias with $\mathrm{SNR} \geq 20$ dB).

The assessment of the minimum QT SD level for which an error tolerance degree of 10%, 15% and 20% was accomplished, for each noise contamination level, was addressed. For that purpose it was checked for data from each QT reference model if the $\varepsilon^{\mathcal{B}}$ quartile box was within the chosen tolerance degree. In Fig. 8(c) is presented, for each dataset and SNR level, the minimum of mean $\hat{\sigma}_{\mathrm{QT}}$ observed in data fulfilling the criteria.

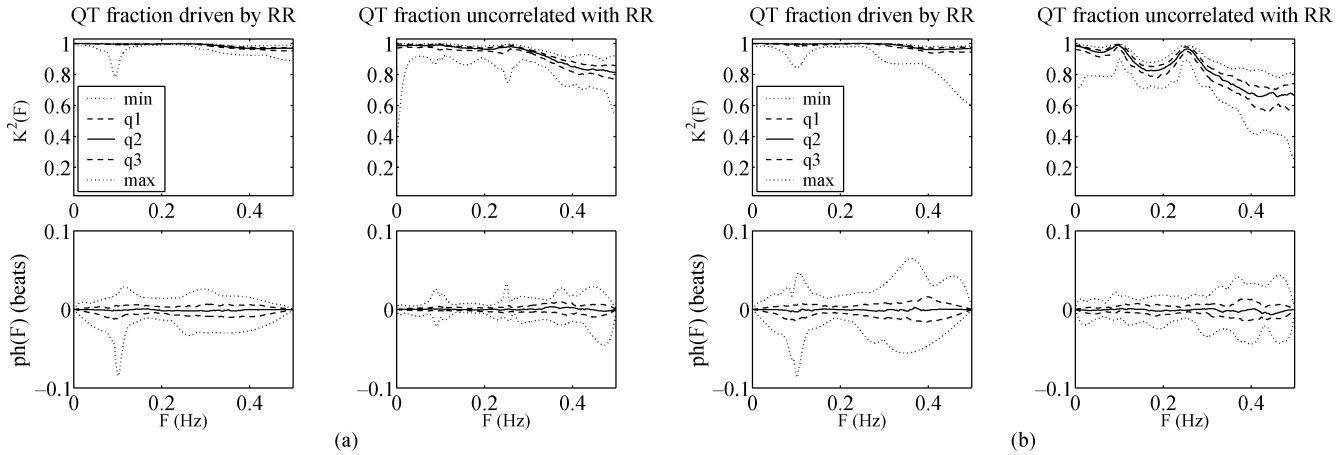

Fig. 7. Similarity between estimated and reference fractions of $x_{\mathrm{QT}}(n)$, right subpanel $x_{\mathrm{QT|RR}}(n)$, left subpanel $x_{\mathrm{QT|QT}}(n)$: minimum (min), first quartile (q1), median (q2), second quartile (q3), and maximum (max) values across trials and along frequency magnitude, of squared spectral coherence, $K^2(F)$, and phase of cross-spectra, $ph(F)$, in data set C_c. Frequency axis assuming uniform heart period T_R. (a) QT reference model Hi; (b) QT reference model Lo.

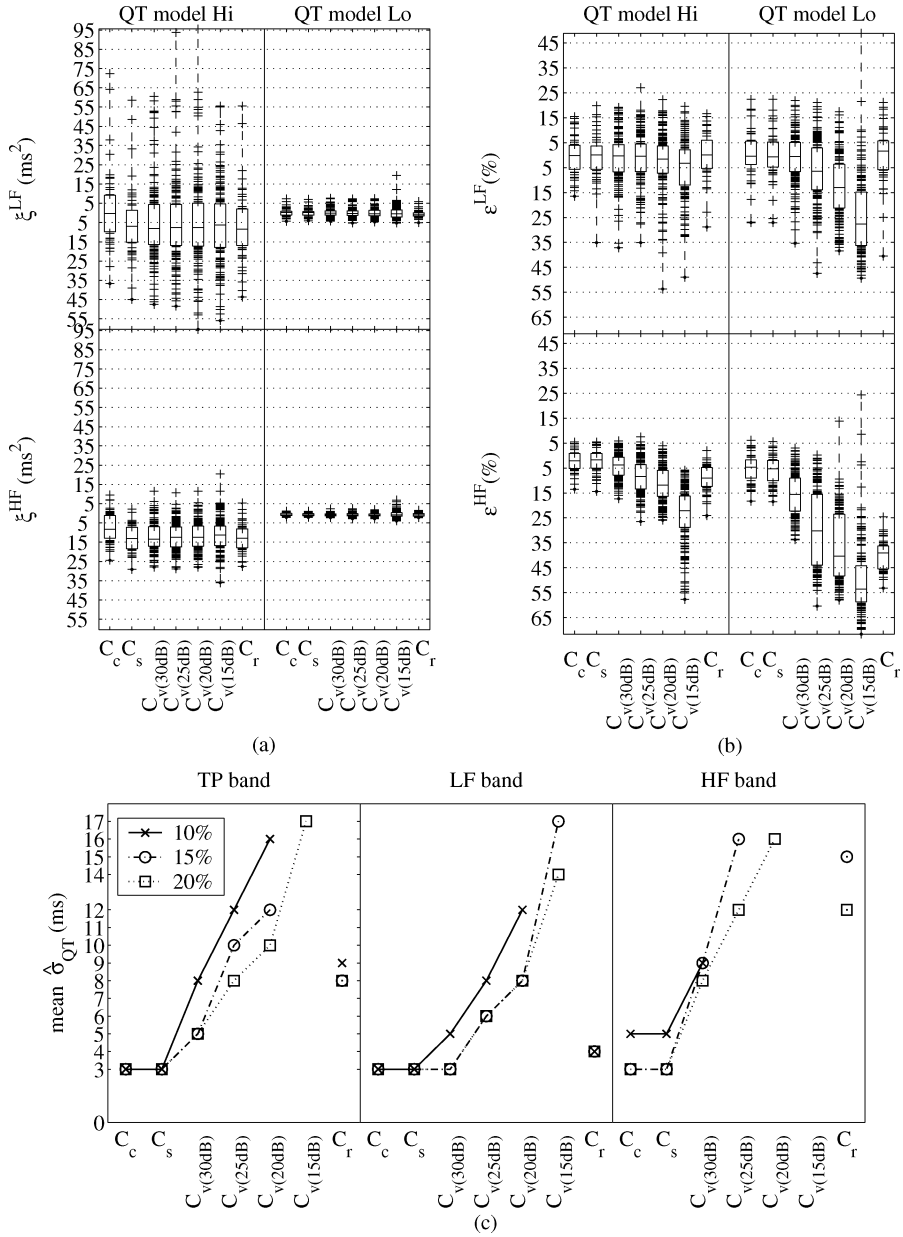

Fig. 8. Distributions of (a) $\xi^{\mathcal{B}}$ and (b) $\varepsilon^{\mathcal{B}}$: box-and-whisker plot by frequency band (stands for values out of the quartiles box). In (c) are plotted the mean $\hat{\sigma}_{\mathrm{QT}}(n)$ observed in each dataset for which $\varepsilon^{\mathcal{B}}$ quartile box is within a tolerance degree of 10%, 15%, and 20%.

TABLE III
REAL DATA SET SEGMENTS DESCRIPTION. $V_{\rm QT} = 100\sigma_{\rm QT}/T_{\rm QT}$

Lead	Segment # (record)	$x_{\rm QT}(n)$ $T_{\rm QT}\pm\hat{\sigma}_{\rm QT}$, ms	$V_{\rm QT}$, %	SNR, dB $mean \pm sd$
X	1(ra2)	327.8±3.0	0.9	21.0 ± 0.6
X	2(ra2)	325.6±3.0	0.9	20.7 ± 0.7
X	3(rb2)	294.2±9.2	3.1	18.6 ± 1.1
X	4(rb2)	302.0±7.8	2.6	19.9 ± 0.8
X	5(rb2)	296.0±8.6	2.9	19.0 ± 1.0
X	6(rb2)	302.6±8.2	2.7	20.9 ± 0.7
X	7(rc2)	347.4±2.4	0.7	24.3 ± 0.7
X	8(re2)	309.0±2.4	0.8	20.6 ± 0.5
X	9(re2)	305.4±2.4	0.8	20.8 ± 0.6
X	10(re2)	303.4±2.2	0.7	20.8 ± 0.5
X	11(rf1)	339.6±2.4	0.7	23.3 ± 0.4
X	12(rf1)	335.6±2.4	0.7	23.2 ± 0.4
X	13(rf2)	356.2±3.4	1.0	22.5 ± 0.9
X	14(rh1)	400.4±11.8	2.9	26.5 ± 1.4
Z	15(ra2)	338.4±4.4	1.3	22.1 ± 0.9
Z	16(ra2)	337±4.6	1.4	22.0 ± 0.7
Z	17(ra2)	330.4±4.2	1.3	21.0 ± 0.5
Z	18(rb2)	294.6±4.6	1.6	24.1 ± 0.5
Z	19(rb2)	295.8±4.4	1.5	24.1 ± 0.6
Z	20(rb2)	299.0±4.4	1.5	23.8 ± 0.6
Z	21(rf1)	340.2±8.0	2.4	25.8 ± 0.5
Z	22(rg1)	353.4±2.8	0.8	24.7 ± 0.7
Z	23(rg1)	356.6±3.2	0.9	25.0 ± 0.9
Z	24(rg3)	349.8±33.4	9.5	15.9 ± 1.9

Notice that values for mean $\hat{\sigma}_{\rm QT}$ are presented for a dataset or SNR level only if data from at least one QT reference model fulfilled the criteria.

B. Real Data

Segments with valid measured series were found for 7 records in lead X and 5 records in lead Z, out of the 20 records available in the real database. There were not any segments qualified in lead Y. A total of 24 segments were analyzed, as summarized in Table III, with several segments in the same file. The SD ($\hat{\sigma}_{\rm QT}$) of $x_{\rm QT}(n)$ in those segments varied mostly from 2 to 12 ms, with a maximum variation coefficient ($V_{\rm QT} = 100\hat{\sigma}_{\rm QT}/T_{\rm QT}$) of 3.1. The exception is the segment 24 which presents much larger values both for $\hat{\sigma}_{\rm QT}$ and $V_{\rm QT}$ (more than the double of the maximum for all the other segments). The minimum SNR mean value found was 15.9 dB again for segment 24; for all other segments SNR values found were higher than 18.5 dB. No valid AR model was found for the $x_{\rm RR}(n)$ in segment 5 of lead Z. The orders selected by AIC in AR indentification [Fig. 5(c)] were found to be $8 \leq p \leq 13$ for 19 segments and in ARARX [Fig. 5(d)] $5 \leq q \leq 10$ for 20 over the remaining 23 segments. Only in 3 out of the 24 segments was found $p = q$.

The estimated QTV fractions are presented in Fig. 9: $R^{\rm LF}_{\rm QT|RR} < 60\%$ for 19 out of 23 segments, the maximum of $R^{\rm HF}_{\rm QT|RR}$ is 64.8%, and $R^{\rm LF}_{\rm QT|RR} > R^{\rm HF}_{\rm QT|RR}$ for 15 of the segments.

VI. DISCUSSION

Restrictive criteria for considering valid interval measures were used, aiming to guaranty that the parametric methods are only applied to data that can be considered as close as possible to stationarity, an essential restriction for this class of methods. In data facing higher noise levels this resulted in a low number of segments qualified for the analysis. For many records in real data, it was not possible to find segments with valid interval measures in any of the available leads and the lead Y (usually noisier and thus likely to present more outliers) had no qualified segments at all.

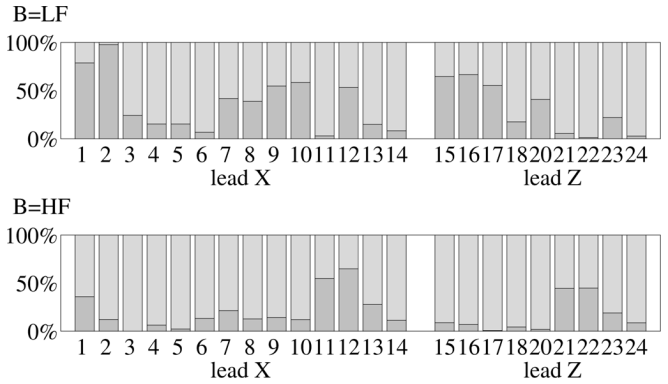

Fig. 9. QTV fractions estimated in real records segments: HRV driven fraction in darker grey, uncorrelated fraction in lighter.

Adequate model identification was possible for more than 90% of the analyzed segments (both simulated and real). The QT reference models used in the simulation allowed to produce $x_{\rm QT}(n)$ series resulting from $x_{\rm RR}(n)$ and other uncorrelated source. In the simulated data sets outliers exclusion in the QT series was not considered, as they can result from the simulation itself instead of delineation errors, since the models do not guarantee fully realistic series in a physiological sense. The orders selected for modelling the majority of the clean simulated series $x_{\rm RR}(n)(5 \leq p \leq 9)$ and the ARARX models $(3 \leq q \leq 7)$ are in accordance with the reference orders ($p = 7$, $q = 4$) used in simulation. In data set A_c, the QTV fraction uncorrelated to HRV is null and, therefore, all the relevant memory effect is included in AR model part: the ARARX part tries to model white noise and selects more spread out orders. In the real data set segments, AIC selected mainly $p > q$ reinforcing the adequacy of allowing different orders for AR and ARARX models. In fact, there is no reason to constrain the QT and RR sequences to attached memories of its own past. Mean value of $\hat{\sigma}_{\rm QT}$ in data set C_c is near $\sigma_{\rm QT}$ for all QT reference models. The lower $\hat{\sigma}_{\rm QT}$ values in data sets A_c and B_c were expected, as only one of the QT dependencies (one QTV fraction) was included.

The errors $\varepsilon^{\mathcal{B}}$ found in the quantification of the QTV fraction driven by HRV over clean simulated series were low for all data sets, indicating that the parametric method is able to correctly estimate both QTV fractions. Higher dispersion and bias of $\varepsilon^{\mathcal{B}}$ were found for QT reference models with lower $\sigma_{\rm QT}$. This effect was expected as the QTV amounts to be estimated were smaller and thus the delineation errors proportionally assumed higher importance. The high $K^2(F)$ between estimated and reference fractions reflect the degree of similarity found both in power and in the peaks location. Erroneous QTV due to delineation errors should be considered as noncorrelated with HRV, explaining the slightly inferior $K^2(F)$ in this fraction, namely in QT reference models with lower $\sigma_{\rm QT}$. The negligible $ph(F)$ values confirm the absence of time delays in the dependence of $x_{\rm QT}(n)$ on $x_{\rm RR}(n)$.

The mean values of $\hat{\sigma}_{\mathrm{QT}}$ in data sets A_s, B_s and C_s differ less than one sample from the correspondent values in A_c, B_c and C_c and no relevant differences were noticed in performance, coherence or phase. The adequateness of the RR and QT intervals measured by the automatic delineator presented in [23] for studying these relations was then confirmed. The slightly lower performance found for QT reference models with $\sigma_{\mathrm{QT}} < 8\,\mathrm{ms}$, can be related not only with the lower QTV levels to be measured, but also with insufficient ECG time resolution (2 ms) resulting from the sampling rate chosen ($F_s = 500\,\mathrm{Hz}$). Still, negligible effects of F_s in the QT interval measurement were found by Risk *et al.* [39], for F_s values between 300 and 500 Hz. By looking the tendencies shown in that work, one can infer than same negligible differences will be found for $F_s \geq 500\,\mathrm{Hz}$.

The negative bias found in $\varepsilon^{\mathcal{B}}$ for C_r, with no relevant performance decrease in $\xi^{\mathcal{B}}$, represents an overestimation of the QTV fraction not correlated with RR. The waves slope is affected by the beat rotation resulting in cyclic delineation errors, with impact in the QTV series. These small delineation errors are consistent with $P^{\mathcal{B}}_{\mathrm{QT|QT}}$ overestimation, specially for $\mathcal{B} = \mathrm{HF}$, which assume relative higher importance for lower QTV levels. The parametric method was inapplicable with noise contamination corresponding to $\mathrm{SNR} < 15\,\mathrm{dB}$ due to the number of outliers in $x_{\mathrm{RR}}(n)$ and missing QT intervals resulting from delineation errors. The progressively increased $\hat{\sigma}_{\mathrm{QT}}$ mean with the SNR reduction in the qualified segments strongly indicated that delineation errors have introduced spurious variability in the measured series. A delineation improvement is needed to allow a faithful QTV estimation in noisier ECG records. As expected, the joint performance of delineation and parametric approach depended not only on the noise level, but also on the QTV level to be measured. In the presence of moderate noise, the quality of the $P^{\mathcal{B}}_{\mathrm{QT|RR}}$ estimation decreased with SNR level, but not to unusable levels, as far as the level of QTV to be measured is not too low ($\hat{\sigma}_{\mathrm{QT}} > 10\ \mathrm{ms}$). Spurious QTV resulting from noise was correctly quantified as not related with RR. Thus, the ratio underestimated the importance of $P^{\mathcal{B}}_{\mathrm{QT|RR}}$ in total QTV and the quantification of the relative fraction of variability driven by RR ($R^{\mathcal{B}}_{\mathrm{QT|RR}}$) was more affected than the absolute measures. The results outlined in Fig. 8 provide, for the used delineation system [23], the limits for which the QTV fraction quantification is reliable, as a function of SNR and QTV range. Those limits would surely be less restrictive if the RTapex [19] was used, since T peak estimation is less noise sensitive, but the eventual variability of the T peak to T end interval (and its potential clinical value) would be lost. The limits found could be even pushed forward by exploring a more robust delineator [40].

Regarding the real data set, the fraction uncorrelated with HRV was found to be higher than 40% for most of the segments for all frequency bands considered, suggesting that other factors rather than RR could drive an important part of QTV. It is worthwhile to remark that uncorrelation between that part of QTV and HRV does not imply the absence of physiological dependence between them, since nonlinear effects are not considered in the present modelling. As SNR level is around 20 dB and $\hat{\sigma}_{\mathrm{QT}}$ SD is $\leq$10 ms for many of the real files, it is likely that the errors in the estimated fractions reach 15% or 20%. Even so, it is possible to state that the fraction uncorrelated with HRV still have a relevant importance in the QTV.

VII. Conclusion

Exploring short term RR and QT interactions in clinical routine data, facing noise contamination, is a challenging and complex problem. In this paper, this relation was assessed by automatic delineation and the characterization of the QT versus RR variabilities using parametric modelling was discussed. The robustness was evaluated with simulated data. No relevant performance decrease resulted from delineation, and the decrease in estimation quality due to ECG noise does not degrade the variability measures to nonuseful levels, with moderate contamination ($\mathrm{SNR} > 15\,\mathrm{dB}$). Noisier ECG records will require an improvement of the delineation system. The level of QTV to be measured is also important in the relevance of the errors. The methods are not adequate to study reduced QTV (QT SD $\leq$10 ms). In real data, the different orders selected for the two model parts can be associated to differences in the memory of the series and need a deeper analysis.

In spite of the limitations in this methodology, the fraction uncorrelated with HRV was found to have an importance in QTV that cannot be ignored. Clinical interpretation studies on the uncorrelated fraction and its possible relation with direct autonomic effects over the VR should be considered and can now be faced within the framework of this modelling.

References

[1] F. Gaita, C. Giustetto, F. Bianchi, C. Wolpert, R. Schimpf, R. Riccardi, S. Grossi, E. Richiardi, and M. Borggrefe, "Short QT syndrome a familial cause of sudden death," *Circulation*, vol. 108, pp. 965–970, 2003.

[2] Y. G. Yap and A. J. Camm, "Drug induced QT prolongation and torsades de pointes," *Heart*, vol. 89, pp. 1363–1372, 2003.

[3] M. Rubart, "Congenital long QT syndrome: looking beyond the heart," *Heart Rhythm*, vol. 1, no. 1, pp. 65–66, 2004.

[4] J. Lass, J. Kaik, D. Karai, and M. Vainu, "Ventricular repolarization evaluation from surface ECG for identification of the patients with increased myocardial electrical instability," *Proc. 23rd Annu. Int. Conf. IEEE Engineering in Medicine and Biology Society*, 2001, pp. 390–393.

[5] S. Cuomo, F. Marciano, M. L. Migaux, F. Finizio, E. Pezzella, M. A. Losi, and S. Betocchi, "Abnormal QT interval variability in patients with hypertrophic cardiomyopathy. Can syncope be predicted?," *J. Electrocardiol.*, vol. 37, no. 2, pp. 113–119, 2004.

[6] R. D. Berger, "QT variability," *J. Electrocardiol.*, vol. 36 suppl., no. 5, pp. 83–87, 2003.

[7] V. K. Yeragani, S. Adiga, N. Desai, and R. D. Berger, "Beat-to-beat QT interval variability in atrial fibrillation with and without congestive cardiac failure," *Ann. Noninvasive Electrocardiol.*, vol. 9, pp. 304–305, 2004.

[8] M. Merri, M. Alberti, and A. J. Moss, "Dynamic analysis of ventricular repolarization duration from 24-hour Holter recordings," *IEEE Trans. Biomed. Eng.*, vol. 40, no. 12, pp. 1219–1225, Dec. 1993.

[9] F. Marciano, S. Cuomo, M. L. Migaux, and A. Vetrano, "Dynamic correlation between QT and RR intervals: how long is QT adaptation to heart rate?," *Comput. Cardiol.*, pp. 413–416, 1998.

[10] V. Shusterman, B. Aysin, S. I. Shah, S. Flanigan, and K. P. Anderson, "Autonomic nervous system effects on ventricular repolarization and RR interval variability during head-up tilt," *Comput. Cardiol.*, pp. 717–720, 1998.

[11] V. Shusterman, A. Beigel, S. I. Shah, B. Aysin, R. Weiss, V. K. Gottipaty, D. Schartzman, and K. P. Anderson, "Changes in autonomic activity and ventricular repolarization," *J. Electrocardiol.*, vol. 32 suppl, pp. 185–192, 1999.

[12] A. Gastaldelli, M. Emdin, F. Conforti, S. Camastra, and E. Ferrannini, "Insulin prolongs the QTc interval in humans," *Am. J. Physiol. Regul. Integr. Comp. Physiol.*, vol. 279, pp. R2022–R2025, 2000.
[13] R. M. Colzani, M. Emdin, F. Conforti, C. Passino, M. Scalattini, and G. Iervasi, "Hyperthyroidism is associated with lengthening of ventricular repolarization," *Clin. Endocrinol.*, vol. 55, no. 1, pp. 27–32, 2001.
[14] A. R. Magnano, S. Holleran, R. Ramakrishnan, J. A. Reiffel, and D. M. Bloomfield, "Autonomic nervous system influences on QT interval in normal subjects," *J. Am. Coll. Cardiol.*, vol. 39, no. 11, pp. 1820–1826, 2002.
[15] T. Murabayashi, B. Fetics, D. Kass, E. Nevo, B. Gramatikov, and R. D. Berger, "Beat-to-beat QT interval variability associated with acute myocardial isquemia," *J. Electrocardiol.*, vol. 35, no. 1, pp. 19–25, 2002.
[16] R. D. Berger, E. K. Kasper, K. L. Baughman, E. Marban, H. Calkins, and G. F. Tomaselli, "Beat-to-beat QT interval variability novel evidence for repolarization lability in ischemic and nonischemic dilated cardiomyopathy," *Circulation*, vol. 96, no. 5, pp. 1557–1565, 1997.
[17] C. C. E. Lang, J. M. M. Neilson, and A. D. Flapan, "Abnormalities of the repolarization characteristics of patients with heart failure progress with symptom severity," *Ann. Noninvasive Electrocardiol.*, vol. 9, no. 3, pp. 257–264, 2004.
[18] M. Merri, J. Benhorin, M. Alberti, E. Locati, and A. J. Moss, "Electrocardiographic quantitation of ventricular repolarization," *Circulation*, vol. 80, pp. 1301–1308, 1989.
[19] A. Porta, G. Baselli, E. Caiani, A. Malliani, F. Lombardi, and S. Cerutti, "Quantifying electrocardiogram RT-RR variability interactions," *Med. Biol. Eng. Comput.*, vol. 36, no. 1, pp. 27–34, 1998.
[20] F. Lombardi, A. Colombo, A. Porta, G. Baselli, S. Cerutti, and C. Fiorentini, "Assessment of the coupling between RT_{apex} and RR interval as an index of temporal dispersion of ventricular repolarization," *PACE*, vol. 21, pp. 2396–2400, 1998.
[21] P. P. Davey, "QT interval measurement: Q to T_{Apex} or Q to T_{End}," *J. Intern. Med.*, vol. 246, no. 2, pp. 145–149, 1999.
[22] G. X. Yan and C. Antzelevitch, "Cellular basis for the normal T wave and the electrocardiographic manifestations of the long-QT syndrome," *Circulation*, vol. 98, pp. 1928–1936, 1998.
[23] J. P. Martínez, R. Almeida, S. Olmos, A. P. Rocha, and P. Laguna, "A wavelet-based ECG delineator: evaluation on standard databases," *IEEE Trans. Biomed. Eng.*, vol. 51, no. 4, pp. 570–581, Apr. 2004.
[24] R. Almeida, A. P. Rocha, E. Pueyo, J. P. Martínez, and P. Laguna, "Modelling short term variability interactions in ECG: QT versus RR," in *Computational Statistics 2004*. Prague: Physica-Verlag, 2004, pp. 597–604.
[25] R. Almeida, E. Pueyo, J. P. Martínez, A. P. Rocha, and P. Laguna, "Quantification of the QT variability related to HRV: robustness study facing automatic delineation and noise on the ECG," *Comput. Cardiol*, pp. 769–772, 2004.
[26] L. Ljung, *System Identification Theory for the User*, 2nd ed. Upper Saddle River, NJ: Prentice-Hall PTR, 1999.
[27] E. Pueyo, P. Smetana, M. Malik, and P. Laguna, "Evaluation of QT interval response to marked RR interval changes selected automatically in ambulatory recordings," *Comput. Cardiol.*, pp. 157–160, 2003.
[28] J. Mateo and P. Laguna, "Improved heart rate variability signal analysis from the beat occurrence times according to the IPFM model," *IEEE Trans. Biomed. Eng.*, vol. 47, no. 8, pp. 985–996, Aug. 2000.
[29] S. Johnsen and N. Andersen, "On power estimation in maximum entropy spectral analysis," *Geophysics*, vol. 43, no. 4, pp. 681–690, 1978.
[30] G. Baselli, A. Porta, O. Rimoldi, M. Pagani, and S. Cerutti, "Spectral decomposition in multichannel recordings based on multivariate parametric identification," *IEEE Trans. Biomed. Eng.*, vol. 44, no. 11, pp. 1092–1101, Nov. 1997.
[31] S. L. Marple, *Digital Spectral Analysis With Applications*. : Prentice Hall, 1987.
[32] S. Waele and P. M. T. Broersen, "Order selection for vector autoregressive models," *IEEE Trans. Acoust., Speech, Signal Process.*, vol. 51, no. 2, pp. 427–433, Feb. 2003.
[33] T. F. of the ESC/ASPE, "Heart rate variability: standards of measurement, physiological interpretation, and clinical use," *Eur. Heart J.*, vol. 17, pp. 354–381, 1996.
[34] B. T. Jensen, C. E. Larroude, L. P. Rasmussen, N. H. Holstein-Rathlou, M. V. Hojgaard, E. Agner, and J. K. Kanters, "Beat-to-beat QT dynamics in healthy subjects," *Ann. Noninvasive Electrocard.*, vol. 9, no. 1, pp. 3–11, 2004.
[35] J. Mateo and P. Laguna, "Analysis of heart rate variability in the presence of ectopic beats using the heart timing signal," *IEEE Trans. Biomed. Eng.*, vol. 50, no. 3, pp. 334–343, Mar. 2003.
[36] M. Astrom, H. C. Santos, L. Sornmo, P. Laguna, and B. Wohlfart, "Vectorcardiographic loop alignment and the measurement of morphologic beat-to-beat variability in noisy signals," *IEEE Trans. Biomed. Eng.*, vol. 47, no. 4, pp. 497–506, Apr. 2000.
[37] G. B. Moody and R. G. Mark, "The MIT-BIH arrhythmia database on CD-ROM and software for use with it," *Comput. Cardiol.*, pp. 185–188, 1990.
[38] F. Pinciroli, G. Pozzi, P. Rossi, M. Piovosi, A. Capo, R. Olivieri, and M. Della Torre, "A respiration-related EKG database," *Comput. Cardiol.*, pp. 477–480, 1998.
[39] M. R. Risk, J. S. Bruno, M. Llamedo Soria, P. D. Arini, and R. A. M. Taborda, "Measurement of QT interval and duration of the QRS complex at different ECG sampling rates," *Comput. Cardiol.*, pp. 495–498, 2005, to be published.
[40] R. Almeida, J. P. Martínez, A. P. Rocha, S. Olmos, and P. Laguna, "Improved QT variability quantification by multilead automatic delineation," *Comput. Cardiol.*, pp. 503–506, 2005.

Rute Almeida was born in Porto, Portugal, in 1979. She received a 4-year degree in mathematics applied to technology in 2000 from Faculty of Sciences, University of Porto (FCUP), Porto. Since October of 2001, she is working towards the Ph.D. degree at the Applied Mathematics Department of FCUP.

She was with the Autonomic Function Study Center from Hospital S. João between March and October 2000, working in methods for automatic delineation of the ECG. She is currently a member of Centro de Matemática da Universidade do Porto and an Invited Assistant in the Mathematics Department of Minho University (Portugal). Her main research interests are in time-scale methods and the automatic analysis of the ECG, namely the study of ventricular repolarization.

Sónia Gouveia was born in Leiria, Portugal, in 1977. She received the 4-year degree in mathematics applied to technology and the M.Sc. degree in computational methods in sciences and engineering from the University of Porto, Porto, Portugal. Since March of 2005, she is working towards the Ph.D. degree in applied mathematics, supported by an individual Ph.D. degree grant from Foundation for Science and Technology (Portugal) and European Social Fund.

From 1999 to 2003, she was with the Autonomic Function Study Center from Hospital S. João, working in methods for automatic processing of biomedical signals and for data analysis in autonomic dysfunction diseases. Currently, she is with the Centro de Matemática da Universidade do Porto as a Researcher. Her main research interests are signal processing techniques for the characterization of biomedical signals.

Ana Paula Rocha (M'02) was born in Coimbra, Portugal, in 1957. She received the Applied Mathematics degree and the Doctor degree (Ph.D. degree in applied mathematics, systems theory, and signal processing) from the Faculty of Sciences, University of Porto (FCUP), Porto, in 1980 and 1993, respectively.

She is an Auxiliar Professor in the Department of Applied Mathematics at FCUP, Portugal. She is currently a member of Centro de Matemática da Universidade do Porto. Her research interests are in biomedical signals and system analysis (EMG, cardiovascular systems analysis and autonomic nervous system characterization), time-frequency/time-scale signal analysis, point processes spectral analysis, and data treatment and interpretation.

Esther Pueyo received the M.S. degree in mathematics from the University of Zaragoza, Zaragoza, Spain, in 1999. During 2000, she was a research student at the Department of Mathematics, University of Zaragoza, where she developed a minor thesis in the field of calculus.

In 2001, she began the Ph.D. degree studies at the Department of Electronic Engineering and Communications, University of Zaragoza, with a grant supported by the Spanish government.

Currently, she is an Assistant Professor with the Department of Electronic Engineering and Communications, University of Zaragoza. Her research activity lies in the field of biomedical signal processing and her primary interests include the study of heterogeneities in the repolarization period of the electrocardiographic signal.

Juan Pablo Martínez was born in Zaragoza, Aragón, Spain, in 1976. He received the M.S. degree in telecommunication engineering and the Ph.D. degree in biomedical engineering from the University of Zaragoza (UZ), in 1999 and 2005, respectively.

From 1999 to 2000, he was with the Department of Electronic Engineering and Communications, UZ, as a Research Fellow. Since 2000, he is an Assistant Professor in the same department. He is also a Researcher with the Aragon Institute of Engineering Research (I3A), UZ. His professional research activity lies in the field of biomedical signal processing, with main interest in signals of cardiovascular origin.

Pablo Laguna (M'92–SM'06) was born in Jaca (Huesca), Spain, in 1962. He received the M.S. degree in physics and the Ph.D. degree in physic science from the Science Faculty at the University of Zaragoza, Zaragoza, Spain, in 1985 and 1990, respectively. The Ph.D. degree thesis was developed at the Biomedical Engineering Division of the Institute of Cybernetics (U.P.C.-C.S.I.C.) under the direction of P. Caminal.

He is Full Professor of Signal Processing and Communications in the Department of Electrical Engineering at the Engineering School, and a Researcher at the Aragn Institute for Engineering Research (I3A), both at University of Zaragoza. From 1992 to 2005, he was Associated Professor at same university and from 1987 to 1992 he worked as Assistant Professor of Automatic Control in the Department of Control Engineering at the Politecnic University of Catalonia (U.P.C.), Catalonia, Spain, and as a Researcher at the Biomedical Engineering Division of the Institute of Cybernetics (U.P.C.-C.S.I.C.). His professional research interests are in signal processing, in particular applied to biomedical applications.